Preprint:

Mineeva, T., Alaoui, A. El, Hakobyan, H. et al. (2024) Suppression of neutral pion production in deep-inelastic scattering off nuclei with the CLAS detector. [Preprint]

https://doi.org/10.48550/arXiv.2406.04513

Suppression of neutral pion production in deep-inelastic scattering off nuclei with the CLAS detector

T. Mineeva,[1,2,*] W. K. Brooks,[1,2,3,4,5] A. El Alaoui,[1,2] H. Hakobyan,[1,2] K. Joo,[6] J.A. López,[1] O. Soto,[7] P. Achenbach,[4] Z. Akbar,[35] J. S. Alvarado,[28] W.R. Armstrong,[8] M. Arratia,[51] H. Atac,[48] H. Avagyan,[4] C. Ayerbe Gayoso,[55] L. Baashen,[18] L. Barion,[22] M. Bashkanov,[53] I. Bedlinskiy,[36] B. Benkel,[1] F. Benmokhtar,[15] A. Bianconi,[50,27] A.S. Biselli,[16] F. Bossù,[13] S. Boiarinov,[4] K.T. Brinkmann,[42] W.J. Briscoe,[20] V.D. Burkert,[4] T. Cao,[4] R. Capobianco,[6] D.S. Carman,[4] J.C. Carvajal,[18] A. Celentano,[24] P. Chatagnon,[4] V. Chesnokov,[46] T. Chetry,[18,34,40] G. Ciullo,[22,17] P.L. Cole,[32] M. Contalbrigo,[22] G. Costantini,[50,27] A. D'Angelo,[25,45] N. Dashyan,[56] R. De Vita,[24] M. Defurne,[13] A. Deur,[4] S. Diehl,[42,6] C. Djalali,[40,47] R. Dupre,[28] H. Egiyan,[4] L. El Fassi,[34] P. Eugenio,[19] S. Fegan,[53] A. Filippi,[26] G. Gavalian,[4,37] G.P. Gilfoyle,[44] F.X. Girod,[4] A.A. Golubenko,[46] G. Gosta,[27] R.W. Gothe,[47] K.A.Griffioen,[55] L. Guo,[18] K. Hafidi,[8] M. Hattawy,[41,8] F. Hauenstein,[4,41] T.B. Hayward,[6] D. Heddle,[14,4] A. Hobart,[28] M. Holtrop,[37] Y.C. Hung,[41] Y. Ilieva,[47] D.G. Ireland,[52] E.L. Isupov,[46] H.S. Jo,[31] D. Keller,[54] A. Khanal,[18] M. Khandaker,[57] W. Kim,[31] F.J. Klein,[12] V.Klimenko,[6] A. Kripko,[42] V. Kubarovsky,[4] S.E. Kuhn,[41] L. Lanza,[25,45] M. Leali,[50,27] S. Lee,[8] P. Lenisa,[22,17] X. Li,[33] I.J.D. MacGregor,[52] D. Marchand,[28] V. Mascagna,[50,49,27] B. McKinnon,[52] S. Migliorati,[50,27] R.G. Milner,[33] M. Mirazita,[23] V. Mokeev,[4] P. Moran,[33] C. Munoz Camacho,[28] P. Nadel-Turonski,[4] K. Neupane,[47] D. Nguyen,[4] S. Niccolai,[28] G. Niculescu,[30] M. Osipenko,[24] A.I. Ostrovidov,[19] M. Ouillon,[28] P. Pandey,[41] M. Paolone,[38,48] L.L. Pappalardo,[22,17] R. Paremuzyan,[4] E. Pasyuk,[4] S.J. Paul,[51] W. Phelps,[14,20] N. Pilleux,[28] M. Pokhrel,[41] J. Poudel,[4,41] J.W. Price,[9] Y. Prok,[41,54] A. Radic,[1] N. Ramasubramanian,[13] T. Reed,[18] J. Richards,[6] M. Ripani,[24] J. Ritman,[21,29] G. Rosner,[52] F. Sabatié,[13] C. Salgado,[39] S. Schadmand,[21] A. Schmidt,[20,33] R.A. Schumacher,[11] M.Scott,[8] E.V. Shirokov,[46] U. Shrestha,[6] D. Sokhan,[13,52] N. Sparveris,[48] M. Spreafico,[24] S. Stepanyan,[4] I.I. Strakovsky,[20] S. Strauch,[47,20] J.A. Tan,[31] N. Trotta,[6] R. Tyson,[52] M. Ungaro,[4,43] S. Vallarino,[22] L. Venturelli,[50,27] H. Voskanyan,[56] E. Voutier,[28] D.P. Watts,[53] X. Wei,[4] L.B. Weinstein,[41] R. Williams,[53] R. Wishart,[52] M.H. Wood,[10] M. Yurov,[34] N. Zachariou,[53] and M. Zurek[8]

(The CLAS Collaboration)

[1] *Universidad Técnica Federico Santa María, Casilla, 110-V Valparaíso, Chile*
[2] *Center for Science and Technology of Valparaíso 699, Valparaíso, Chile*
[3] *SAPHIR Millennium Science Institute, Santiago, Chile*
[4] *Thomas Jefferson National Accelerator Facility, Newport News, VA 23606*
[5] *Duke University, Durham, NC 27708*
[6] *University of Connecticut, Storrs, CT 06269*
[7] *Universidad de La Serena, 1720170 La Serena, Chile*
[8] *Argonne National Laboratory, Argonne, IL 60439*
[9] *California State University, Dominguez Hills, Carson, CA 90747*
[10] *Canisius College, Buffalo, NY 14208*
[11] *Carnegie Mellon University, Pittsburgh, PA 15213*
[12] *Catholic University of America, Washington, D.C. 20064*
[13] *IRFU, CEA, Université Paris-Saclay, F-91191 Gif-sur-Yvette, France*
[14] *Christopher Newport University, Newport News, VA 23606*
[15] *Duquesne University, 600 Forbes Avenue, Pittsburgh, PA 15282*
[16] *Fairfield University, Fairfield, CT 06824*
[17] *Università di Ferrara, 44121 Ferrara, Italy*
[18] *Florida International University, Miami, FL 33199*
[19] *Florida State University, Tallahassee, FL 32306*
[20] *The George Washington University, Washington, D.C. 20052*
[21] *GSI Helmholtzzentrum für Schwerionenforschung GmbH, D-64291 Darmstadt, Germany*
[22] *INFN, Sezione di Ferrara, 44100 Ferrara, Italy*
[23] *INFN, Laboratori Nazionali di Frascati, 00044 Frascati, Italy*
[24] *INFN, Sezione di Genova, 16146 Genova, Italy*
[25] *INFN, Sezione di Roma Tor Vergata, 00133 Rome, Italy*
[26] *INFN, Sezione di Torino, 10125 Torino, Italy*
[27] *INFN, Sezione di Pavia, 27100 Pavia, Italy*
[28] *Universit'e Paris-Saclay, CNRS/IN2P3, IJCLab, 91405 Orsay, France*
[29] *Institut für Kernphysik (Juelich), Juelich, 52428, Germany*
[30] *James Madison University, Harrisonburg, VA 22807*
[31] *Kyungpook National University, Daegu 41566, Republic of Korea*
[32] *Lamar University, 4400 MLK Blvd, PO Box 10046, Beaumont, TX 77710*

arXiv:2406.04513v2 [hep-ex] 6 Aug 2024

[33] *Massachusetts Institute of Technology, Cambridge, MA 02139-4307*
[34] *Mississippi State University, Mississippi State, MS 39762-5167*
[35] *National Research and Innovation Agency (BRIN), Indonesia*
[36] *National Research Centre Kurchatov Institute - ITEP, Moscow, 117259, Russia*
[37] *University of New Hampshire, Durham, NH03824-3568*
[38] *New Mexico State University, PO Box 30001, Las Cruces, NM 88003*
[39] *Norfolk State University, Norfolk, VA 23504*
[40] *Ohio University, Athens, OH 45701*
[41] *Old Dominion University, Norfolk, VA 23529*
[42] *II Physikalisches Institut der Universitaet Giessen, 35392 Giessen, Germany*
[43] *Rensselaer Polytechnic Institute, Troy, NY 12180-3590*
[44] *University of Richmond, Richmond, VA 23173*
[45] *Università di Roma Tor Vergata, 00133 Rome Italy*
[46] *Skobeltsyn Institute of Nuclear Physics, Lomonosov Moscow State University, 119234 Moscow, Russia*
[47] *University of South Carolina, Columbia, SC 29208*
[48] *Temple University, Philadelphia, PA 19122*
[49] *Università degli Studi dell'Insubria, 22100 Como, Italy*
[50] *Università degli Studi di Brescia, 25123 Brescia, Italy*
[51] *University of California Riverside, 900 University Avenue, Riverside, CA 92521*
[52] *University of Glasgow, Glasgow G12 8QQ, United Kingdom*
[53] *University of York, York YO10 5DD, United Kingdom*
[54] *University of Virginia, Charlottesville, VA 22901*
[55] *College of William and Mary, Williamsburg, VA 23187-8795*
[56] *Yerevan Physics Institute, 375036 Yerevan, Armenia*
[57] *Idaho State University, Pocatello, Idaho 83209*

(Dated: August 8, 2024)

We present the first three-fold differential measurement for neutral pion multiplicity ratios produced in semi-inclusive deep-inelastic electron scattering on carbon, iron and lead nuclei normalized to deuterium from CLAS at Jefferson Lab. We found that the neutral pion multiplicity ratio is maximally suppressed for the leading hadrons (energy fraction $z \to 1$), suppression varying from 25% in carbon up to 75% in lead. An enhancement of the multiplicity ratio at low z and high p_T^2 is observed, suggesting an interconnection between these two variables. This behavior is qualitatively similar to the previous two-fold differential measurement of charged pions by the HERMES Collaboration and recently - by CLAS Collaboration. The largest enhancement was observed at high p_T^2 for heavier nuclei, namely iron and lead, while the smallest enhancement was observed for the lightest nucleus, carbon. This behavior suggests a competition between partonic multiple scattering, which causes enhancement, and hadronic inelastic scattering, which causes suppression.

Hadron formation in scattering processes creates new gravitational mass from pure energy, linking the strong and gravitational interactions. This connection, via the energy-momentum tensor of Quantum Chromodynamics (QCD), has recently been developed [1] and applied to the description of experimental data [2–4], and most recently described with a relativistic treatment on the light front [5, 6]. Hadron formation is one of the last frontiers of QCD. While successful models of this process exist, they only have a tenuous connection to the underlying QCD origin of the process. The long distance scales involved in hadron formation currently preclude use of perturbative methods to calculate, for example, fragmentation functions (FF), which describe how color-carrying quarks and gluons turn into color-neutral hadrons or photons [7].

The kinematic region of lepton deep-inelastic scattering at high x_{Bj}, where x_{Bj} is the fraction of the proton momentum carried by the struck quark, offers a powerfully simple interpretation compared to low x_{Bj} where quark pair production dominates [8]. In the single-photon exchange approximation, a valence quark absorbs the full energy and momentum of the virtual photon γ^*; thus, the energy transfer gives the initial energy of the struck quark, neglecting intrinsic quark momentum, and neglecting Fermi momentum of the nucleon for nuclear interactions. At the same level of approximation, the initial direction of the struck quark is known from the momentum transfer of the collision, which provides a unique reference axis. For nuclear targets, this essentially creates a secondary "beam" of quarks of known energy and direction, for which the interaction with the nuclear system provides information at the femtometer distance scale.

An important experimental observable sensitive to the in-medium hadronization process - the complex process of the evolution of a struck quark into multiple hadrons - is the hadronic multiplicity ratio. It is defined as the normalized yield of hadron h produced on a heavy nuclear target A relative to a light nuclei, e.g., deuterium D:

$$R_h(\nu, Q^2, z, p_T^2) = \frac{N_h^A(\nu, Q^2, z, p_T^2)/N_e^A(\nu, Q^2)}{N_h^D(\nu, Q^2, z, p_T^2)/N_e^D(\nu, Q^2)}, \quad (1)$$

where N_h is the number of hadrons produced in semi-inclusive deep-inelastic scattering (SIDIS) events, in which, following the γ^* scattering off the quark, the leading hadron is detected in addition to the scattered electron; N_e is the number of DIS electrons within the same inclusive kinematic bins for the numerator as for the denominator; Q^2 is the γ^* four-momentum transfer squared, ν is the energy transferred which in the lab frame is defined as $\nu = E - E'$ (E and E' is energy of the incoming and outgoing electrons, respectively), z is the energy fraction of the hadron defined as $z = \mathrm{E}_h/\nu$, and p_T^2 is the component of the hadron momentum squared transverse to the γ^* direction; the dependence on ϕ_{pq}, the azimuthal angle of the hadron with with respect to the lepton plane, was integrated over. The hadronic multiplicity ratio quantifies the extent to which hadron production is enhanced or attenuated in nuclei compared to deuterium; in the absence of any nuclear effects, this observable is equal to unity.

Nuclear SIDIS experiments have been performed in fixed-target conditions in facilities such as SLAC, CERN (SPS), DESY (HERMES) and Jefferson Lab (CLAS). The study of nuclear SIDIS with fully identified final state hadrons began with the HERMES program, which published a series of papers between 2001 and 2011 [9–14], opening an era of quantitative studies of color propagation and hadron formation using nuclei as spatial analyzers. The one- and two-fold hadron production data off nuclei can be described with some level of success by models [15–30] using two in-medium ingredients: (1) quark energy loss and (2) interactions of forming hadrons with the nuclear medium. The final HERMES paper [14] underlines the importance of multi-differential cross sections, since charged-hadron multiplicity data displays nontrivial features that cannot be captured by a one-dimensional description, particularly for the baryons. A comprehensive review can be found in Ref. [31]. One-, two- and three-fold measurements of R_h for identified hadrons were reported by CLAS experiments [32–34].

This paper presents the first multi-dimensional measurement of neutral pion multiplicity ratios in SIDIS kinematics. Neutral pions are substantially more difficult to measure than charged pions due to more limited statistics and due to the presence of combinatorial backgrounds. While having a much more limited range in Q^2 and ν, the integrated luminosity in the new data set is two orders of magnitude greater than that of HERMES, dramatically increasing the statistical accuracy of the measurement. This allowed us to extend one-dimensional HERMES π^0 data measured up to mass number 131 [11], to three-dimensional data with mass numbers up to 208.

The data were collected during the EG2 run period in Hall B of Jefferson Lab using the CEBAF Large Acceptance Spectrometer (CLAS) [35] and a 5.014 GeV electron beam. CLAS was based on a six-fold symmetric toroidal magnet, created by six large superconducting coils that divided the spectrometer into six independently instrumented sectors, and comprised of four types of detectors: drift chambers (DC) followed by Cerenkov counters (CC), time-of-flight (TOF) scintillators, and electromagnetic shower calorimeters (EC). Photons from π^0 decay were measured in the EC at angles from about 8 to 45 degrees.

One key ingredient in reducing systematic uncertainties of the multiplicity ratios was the use of a dual-target. The target system consisted of a 2-cm-long liquid-deuterium cryotarget separated by 4 cm from independently insertable solid targets (see Ref. [36]). The center of the cryotarget cell and the solid target were placed 30 cm and 25 cm upstream of the CLAS center, respectively, in order to increase acceptance for negatively charged particles. The advantage of the double target is that since the electron beam passed simultaneously through both targets, time-dependent systematic effects were reduced. A wealth of information was collected during EG2 experiment providing data for hadronization, color transparency [37] and short-range correlations [38] studies.

The SIDIS reaction $e + A \to e' + \pi^0 + X$ is measured, where e and e' are the incident and scattered electrons, respectively, and X is the undetected part of the hadronic final state. Since the π^0 decays almost instantaneously into two photons ($\pi^0 \to \gamma\gamma$), events with one scattered electron and at least two photons were selected. The invariant mass of the two-photon system was used to identify π^0 candidates.

The scattered electrons were selected in the following ranges: $1.0 < Q^2 < 4.1$ GeV^2, $2.2 < \nu < 4.25$ GeV and $W > 2$ GeV, where W is γ^*-nucleon invariant mass squared. The requirement on $Q^2 > 1$ GeV^2 and $W > 2$ GeV allowed to probe nucleon structure in the DIS regime and reduce nucleon resonance region contributions; the requirement on $\nu < 4.25$ GeV allowed to reduce the size of radiative effects also reflected in $y = \frac{\nu}{E}$ <0.85 cut, where y is the energy fraction of the γ^*. These cuts ensured $x_{Bj} > 0.1$, meaning that valence quarks in the target nucleon were probed. Detector acceptance and experimental statistics dictated π^0 kinematics of $0.3 < z < 1.0$ and $0 < p_T^2 < 1.5$ GeV^2. The event phase space was divided into two sets of three-fold differential multiplicity ratios with: 1) a total of 108 bins in (ν, z, p_T^2) integrated over Q^2, and 2) a total of 54 bins in (Q^2, ν, z) integrated over p_T^2.

The electron selection was done as following: first, a negatively charged track in the DC plus a signal in the TOF and EC was required; next, this candidate must have matching between mirror number and projectile angle of the track in CC (this requirement is similar to the cut on the number of photoelectrons without removing good electrons); it further must satisfy sampling fraction cut and have a minimum energy deposited in EC and, lastly, satisfy a coincidence time cut between the EC and TOF signals. We excluded DC regions with non-

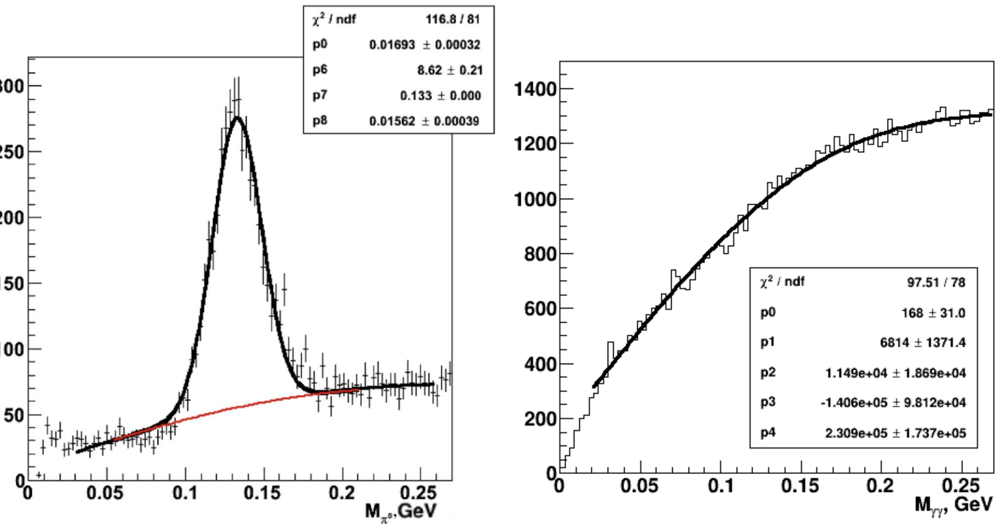

Figure 1. Left: N_{events} versus π^0 invariant mass in a particular (ν, z, p_T^2) bin with fit to a scaled mixed background (red). Right: N_{events} versus invariant mass of the corresponding mixed background fitted with a 4th order polynomial. The total fit function is: p[0]·(p[1]+p[2]·x+p[3]·x^2+p[4]·x^3+p[5]·x^4)+p[6] ·exp($\frac{-(x-p[7])^2}{2\cdot p[8]^2}$), where p_0 is background normalization, p_1-p_5 are predetermined by the event mixing, p_6-p_8 are free parameters corresponding to normalization, μ and σ of the Gaussian peak. The fitting procedure was performed twice: first, in the range $0.03 < M_{\gamma\gamma} < 0.25$ GeV to provide an estimate to μ and σ; second, in the range (-5σ,+5σ) as indicated by the length of the red curve.

uniform tracking efficiency and transverse shower leakage. In order to determine the origin of the scattering event, the intersection of the electron track with the plane containing the ideal beam position was used. However, during the experiment, the beam was offset introducing sector-dependent effects in the vertex reconstruction. Electron-proton elastic scattering was used to determine the beam offset which was then used to correct the reconstructed interaction vertex for each event to make it sector-independent.

Following electron identification, all the neutral hits were considered in the EC provided their energy exceeded 0.3 GeV. Photons were separated from neutrons based on expected photon arrival time $\Delta t = t_{EC}$ - $l_{EC}/30$ - t_{start}, where t_{EC} is time at the EC in ns, l_{EC} is the distance from the target to the EC hit in cm, the speed of light is 30 [cm/ns] and t_{start} is the event start time [39]. To avoid transverse shower energy leakage, events at the edge of the EC were rejected. Photons detected within 12° of the electron track were rejected in order to remove events from bremsstrahlung radiation. In order to improve π^0 resolution, measured photon energy was corrected for a small momentum dependence of the EC sampling fraction [39]. Finally, π^0 candidates were reconstructed from all pairs of photons detected in each event (see Fig. 1). After photon energy correction, the minimum energy of π^0 candidate was E_{π^0} >0.5 GeV.

To calculate the number of π^0's, the two-photon invariant mass spectrum was fit with a Gaussian function plus a polynomial background (see Fig. 1). To determine the shape of combinatorial background, an event mixing technique, consisted of combining photons from uncorrelated events was used. In order to achieve good description of the backgrounds across all kinematics, only photons from kinematically matched events were combined. A detailed description of the improved event-mixing technique can be found in Ref. [39]. The number of π^0's was calculated from the integral of the Gaussian function situated on top of 4th-order polynomial of the event-mixed background.

The multiplicity ratio of Eq. 1 can be viewed as π^0 number ratio $N_{\pi^0}^{A/D}$ normalized by the electron number ratio $N_e^{D/A}$. Corrections to $N_e^{D/A}$ include: (i) acceptance correction factors: these range from unity up to 8%; (ii) radiative corrections due to internal radiation associated with bremsstrahlung off the nucleon: increase the multiplicity ratio up to 3%; (iii) radiative corrections due to Coulomb distortion in the field of the nucleus: decrease the multiplicity ratio down to 4% with the largest corrections for Pb. Internal radiative corrections were calculated based on the Mo and Tsai formalism [40] while Coulomb corrections - on the effective momentum approximation [41]. Both are incorporated in the EXTERNAL code [42]. Additionally, the external radiative corrections that are associated with bremsstrahlung in the target material were incorporated in the GEANT3 simulations, and were accounted for by applying acceptance correction factors.

Corrections applied to the $N_{\pi^0}^{A/D}$ include: (i) acceptance correction factors: these change the multiplicity ratio from -17% to +8% for (ν, z, p_T^2) bins and from -14% to +4% for (Q^2, ν, z); (ii) radiative corrections for SIDIS

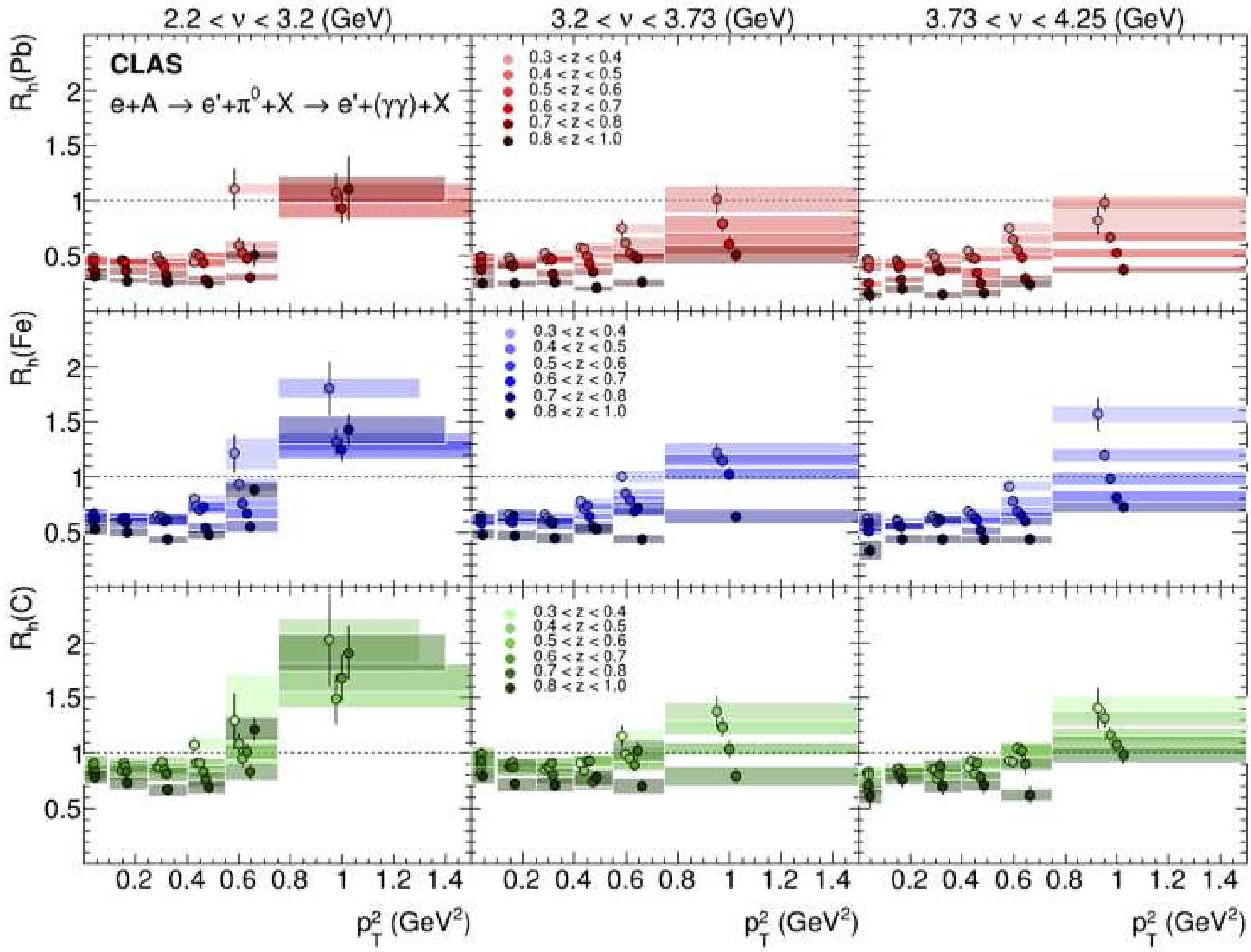

Figure 2. π^0 multiplicity ratios for C, Fe, and Pb in (ν, z, p_T^2) bins plotted as a function of p_T^2 in bins of ν (top horizontal line) and z (indicated by the color). Points are shifted for ease of visualization around the mean value of p_T^2. Statistical uncertainties are indicated by black vertical lines; systematic uncertainties by the color bars. Horizontal uncertainties are related to the size of the bin: while for most bins in p_T^2 they are the same for each bin in z and target, a few bins have smaller uncertainty bands related to the interval of data significance in the bin.

π^0: these affect the multiplicity ratio by less than 0.5%. The latter were calculated using HAPRAD code [43] that was modified using empirically derived nuclear structure functions. The combined effect of $N_e^{D/A}$ and $N_{\pi^0}^{A/D}$ radiative corrections does not exceed 4.8%. Finally, due to the presence of the 15 μm aluminum walls (endcaps) of the liquid-deuterium target cell, we corrected multiplicity ratio for the N_e^D and $N_{\pi^0}^D$ resulting in less than 1% correction.

Acceptance correction factors were calculated on a bin-by-bin basis using the LEPTO event generator 6.5.1 [44], modified to include nuclear Fermi motion of the target nucleon according to the Ciofi-Simula parametrization [45]. The CLAS detector response was simulated with the GSIM package, based on GEANT3, which includes the locations and materials of the dual-target.

Systematic uncertainties of the measurement are comprised of the following: (i) electron identification: target selection cuts, EC sampling fraction cuts, π^- contamination, DC fiducial cuts, and electron radiative corrections; (ii) photon identification: cut on minimum energy deposited in EC, time cut Δt, EC fiducial cuts; and (iii) π^0 identification: background and signal shapes of the invariant mass distribution, acceptance corrections, and SIDIS radiative corrections. Systematic uncertainties were evaluated independently for each set of bins, (ν, z, p_T^2) or (Q^2, ν, z), for each nuclear ratio and applied either as a normalization or as a bin-by-bin uncertainty. The largest contribution to the normalization-type uncertainty came from target vertex identification. It results

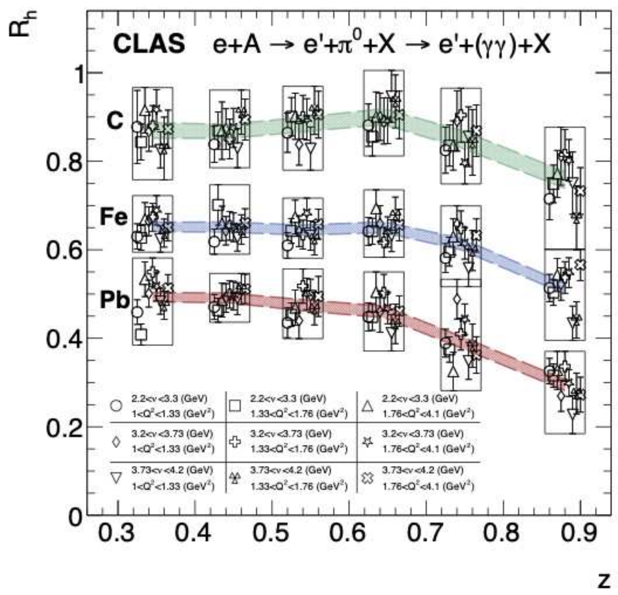

Figure 3. π^0 multiplicity ratios for C, Fe, and Pb in (Q^2, ν, z) bins plotted as a function of z. Each one of the six bins in z contains 9 points corresponding to the 3 bins of ν and 3 bins in Q^2. Each of the 9 points in z is shifted around the center value of the bin; the points, plotted together with its statistical and systematic uncertainties, are enclosed in a box to improve the visualization. The center of the box is the center of the z bin, and the outermost uncertainty of each set defines the height of the box. Additionally, for the purpose of visualization, each target has a band drawn around the average with the width corresponding to the average of all measurements performed in each z-bin.

in 3.1%, 2.4% and 2.3%, for C, Fe and and Pb, respectively, in the (ν, z, p_T^2) set of bins, and slightly smaller values for the (Q^2, ν, z) bins. The dominant source of the bin-by-bin systematic uncertainty is the π^0 invariant mass fit. This uncertainty included both uncertainties on the background and signal shapes ranging on average from 1.4% for Fe in (Q^2, ν, z) bins to 4.7% for Pb in (ν, z, p_T^2) bins. The total average systematic uncertainties in (Q^2, ν, z) are 5.0%, 4.9% and 6.9% for C, Fe and Pb multiplicities correspondingly; in (ν, z, p_T^2) they average to 7.1%, 7.1% and 9.6% for C, Fe and Pb, respectively. The average statistical uncertainty is typically several percent less.

The three-fold π^0 multiplicity ratios are presented in bins of (ν, z, p_T^2) integrated over Q^2 (Fig. 2) and in bins of (Q^2, ν, z) integrated over p_T^2 (Fig. 3). In Fig. 3 multiplicity ratios, presented as a function of z in bins of (Q^2, ν), show flat behavior in the range $0.3 < z < 0.65$ and monotonic decrease for higher z. The dependence on nuclear size suggests a path length-dependent process: for the smallest nucleus, carbon, suppression ranges from approximately 10% for moderate z to about 25% at the highest z. In contrast, for the largest nucleus, lead, suppression ranges from 50% up to approximately 75% at the highest z. In modern versions of energy loss models [46], this attenuation is attributed to the assumption that the propagating quark emits multiple gluons as it transverses the nuclear medium; the larger the nucleus, the greater the gluon emission and quark energy losses are. In the framework of the GiBUU (Giessen Boltzmann-Uehling-Uhlenbec) transport model [17], largely based on elastic and inelastic pre-hadronic final-state interactions, overall attenuation is understood in terms of pure hadron absorption due to increased interaction time with the nuclear medium. One model invoking interference processes gave qualitative indications that quantum mechanical effects could also play a role [15]. From Fig. 3, no effective dependence on energy and momentum transfer to the system, *i.e*, Q^2 and ν, is observed. Range of CLAS kinematics is, however, much less than that of HERMES, where such dependencies were observed.

In Figure 2 multiplicity ratios are presented as a function of p_T^2 in bins of (ν, z). The global trend for all three targets is the enhancement of R_h at high p_T^2 while an overall decrease with increasing z. R_h has a pronounced dependence on p_T^2 in correlation with z: it is independent of p_T^2 for all values of z providing $p_T^2 < 0.5$ GeV^2, however, it increases rapidly for large p_T^2 and small z to the values exceeding unity. The nuclear ordering of R_h enhancement at high p_T^2 compared to low p_T^2 shows that the enhancement is the largest for heavier nuclei, lead and iron, while the smallest relative enhancement is observed for carbon. Additionally, there is a clear dependence on ν with the enhancement being the largest at the lowest values ν.

The pattern of R_h enhancement at low z and high p_T^2 is often referred to as Cronin effect [47]. It was first observed in the measurements by European Muon Collaboration (EMC) [48], Fermilab E665 experiment [49], and further confirmed by HERMES [14] and CLAS [34] measurements. The R_h behavior reported in this paper is qualitatively similar to the previous HERMES and CLAS measurements on charged pions. Theoretically, the Cronin effect is explained by multiple parton scatterings that occur before its fragmentation into final state hadrons. In the limit $z \to 1$, the lifetime of the propagating quark vanishes as it is not allowed to lose any energy and, thus, cannot accumulate transverse momentum through re-scattering. On the other hand, the low z regime pertains to the opposite behavior that leads to the enhancement of transverse momenta. Such a scenario also suggests that the attenuation in the limit $z \to 1$ is purely due to hadron absorption. The dependence of the Cronin effect on the nuclear size points to a competition between partonic multiple scattering, which causes enhancement, and hadronic inelastic scattering, which causes suppression.

In summary, we present the first differential π^0 multiplicity ratios measurement produced in SIDIS off D, C, Fe and Pb. The results are reported in two sets of bins: $R_h(Q^2,\ \nu,\ z)$ and $R_h(\nu,\ z,\ p_T^2)$. From the first set of bins, we observe that the ratios depend strongly on nuclear size showing the largest suppression for the highest atomic number A. This suppression is constant for moderate z range and decreases rapidly for leading hadrons ($z > 0.65$); the maximum suppression varies from 25% on carbon to 75% on lead. On the kinematical range of CLAS experiment, suppression of neutral pions did not show dependence on energy and momentum transfer to the system, *i.e* ν and Q^2. The second set of bins shows that multiplicity ratios are enhanced above unity for large p_T^2 and small z (Cronin effect). The nuclear ordering of the Cronin effect shows that the most significant enhancement at high p_T^2 occurs for the heaviest nuclei, such as iron and lead. Additionally, there is a noticeable dependence on ν, with the largest Cronin effect observed at the lowest energy transfers.

These measurements have been successfully extended with an 11 GeV electron beam in the Jefferson Lab experiment E12-06-117 [50]. Offering a wider range in Q^2 and ν and higher luminosity, a wealth of new opportunities is becoming feasible: access to the quark mass dependence of the hadronization with GeV-scale meson formation, extraction of four-fold multiplicities for a large spectrum of hadrons, and searches for diquark correlations in baryon formation [33, 51]. With its collider energies and extended range of kinematic variables, the proposed eA program at the Electron-Ion Collider [52] will provide new insights into hadronization mechanisms. This includes clean measurements of medium-induced energy loss in scenarios where hadrons are formed outside the nuclear medium, as well as studies of potentially very different hadronization properties for heavy mesons.

ACKNOWLEDGEMENTS

The authors would like to thank Dave Gaskell for fruitful discussions on radiative corrections with EXTERNAL code. We acknowledge the staff of the Accelerator and the Physics Divisions at Jefferson Lab in making this experiment possible. This work is supported by the Chilean Agencia Nacional de Investigacion y Desarollo (ANID), FONDECYT grants No.11181215 and No.1221827, No.1161642 and No.1240904, ANID PIA/APOYO AFB230003, and by the ANID-Millennium Science Initiative Program - ICN2019_044. This work was supported in part by the U.S. Department of Energy (DOE) and National Science Foundation (NSF), the Italian Istituto Nazionale di Fisica Nucleare (INFN), the French Centre National de la Recherche Scientifique (CNRS), the French Commissariat á l'Energie Atomique (CEA), the Skobeltsyn Institute of Nuclear Physics (SINP), the Scottish Universities Physics Alliance (SUPA), the National Research Foundation of Korea (NRF), the UK Science and Technology Facilities Council (STFC). The Southeastern Universities Research Association (SURA) operates the Thomas Jefferson National Accelerator Facility for the U.S. Department of Energy under Contract No. DE-AC05-06OR23177.

* mineeva@jlab.org

[1] M. V. Polyakov and P. Schweitzer, International Journal of Modern Physics A **33**, 1830025 (2018).
[2] V. Burkert, L. Elouadrhiri, and F. Girod, Nature **557**, 396 (2018).
[3] K. Kumerički, Nature **570**, E1 (2019).
[4] H. Dutrieux, C. Lorcé, H. Moutarde, P. Sznajder, A. Trawiński, and J. Wagner, Eur. Phys. J. C **81**, 300 (2021), arXiv:2101.03855 [hep-ph].
[5] A. Freese and G. A. Miller, Physical Review D **103** (2021), 10.1103/physrevd.103.094023.
[6] A. Freese and G. A. Miller, "Genuine empirical pressure within the proton," (2021), arXiv:2104.03213 [hep-ph].
[7] A. Metz and A. Vossen, Progress in Particle and Nuclear Physics **91**, 136 (2016).
[8] V. Del Duca, S. J. Brodsky, and P. Hoyer, Phys. Rev. D **46**, 931 (1992).
[9] A. Airapetian, H. Bulten, W. Hesselink, A. Laziev, J. Martin, F. Schmidt, M. Simani, E. Thomas, J. van den Brand, and J. de Visser, European Physical Journal C. Particles and Fields **20**, 479 (2001).
[10] A. Airapetian *et al.* (HERMES Collaboration), Physics Letters B **577**, 37 (2003).
[11] A. Airapetian *et al.* (HERMES Collaboration), Nucl. Phys. B **780**, 1 (2007), arXiv:0704.3270 [hep-ex].
[12] A. Airapetian *et al.* (HERMES Collaboration), Phys. Rev. Lett. **96**, 162301 (2006), arXiv:hep-ex/0510030.
[13] A. Airapetian *et al.* (HERMES Collaboration), Phys. Lett. B **684**, 114 (2010), arXiv:0906.2478 [hep-ex].
[14] A. Airapetian *et al.* (HERMES Collaboration), Eur. Phys. J. A **47**, 113 (2011), arXiv:1107.3496 [hep-ex].
[15] B. Kopeliovich, J. Nemchik, E. Predazzi, and A. Hayashigaki, Nuclear Physics A **740**, 211–245 (2004).
[16] B. Guiot and B. Z. Kopeliovich, Physical Review C **102**, 094023 (2020).
[17] K. Gallmeister and U. Mosel, Nuclear Physics A **801**, 68–79 (2008).
[18] T. Falter, W. Cassing, K. Gallmeister, and U. Mosel, Acta Physica Hungarica A) Heavy Ion Physics **27**, 71–78 (2006).
[19] T. Falter, W. Cassing, K. Gallmeister, and U. Mosel, Physical Review C **70**, 045201 (2004).
[20] T. Falter and U. Mosel, Fizika B **13**, 165 (2004), arXiv:nucl-th/0308073.
[21] T. Falter, W. Cassing, K. Gallmeister, and U. Mosel, Physics Letters B **594**, 61–68 (2004).
[22] X.-N. Wang, Nuclear Physics A **702**, 238–248 (2002).
[23] J. Osborne and X.-N. Wang, Nuclear Physics A **710**, 281–302 (2002).
[24] N.-B. Chang, W.-T. Deng, and X.-N. Wang, Physical Review C **89**, 54609 (2014).

[25] A. Majumder, E. Wang, and X.-N. Wang, Phys. Rev. Lett. **99**, 152301 (2007).
[26] B.-W. Zhang, X.-N. Wang, and A. Schäfer, Nuclear Physics A **783**, 551–554 (2007).
[27] X.-N. Wang, Nuclear Physics A **702**, 238–248 (2002).
[28] Z.-B. Kang, E. Wang, X.-N. Wang, and H. Xing, Physical Review D **94**, 34911 (2016).
[29] B. Z. Kopeliovich, H.-J. Pirner, I. K. Potashnikova, I. Schmidt, A. V. Tarasov, and O. O. Voskresenskaya, Physical Review C **78**, 114024 (2008).
[30] W. K. Brooks and J. A. López, Physics Letters B **816**, 136171 (2021).
[31] A. Accardi, F. Arleo, W. K. Brooks, D. D'enterria, and V. Muccifora, La Rivista del Nuovo Cimento **32**, 439–554 (2009).
[32] A. Daniel *et al.* (CLAS Collaboration), Phys. Lett. B **706**, 26 (2011), arXiv:arXiv:1111.2573 [nucl-ex].
[33] T. Chetry, L. El Fassi, *et al.* (CLAS Collaboration), Phys. Rev. Lett. **130**, 142301 (2023).
[34] S. Moran *et al.* (CLAS Collaboration), Phys. Rev. C **105**, 015201 (2022), arXiv:2109.09951 [nucl-ex].
[35] B. A. Mecking *et al.*, Nucl. Instrum. Meth. A **503**, 513 (2003).
[36] H. Hakobyan *et al.*, Nuclear Instruments and Methods in Physics Research Section A: Accelerators, Spectrometers, Detectors and Associated Equipment **592**, 218 (2008).
[37] L. El Fassi *et al.* (CLAS Collaboration), Phys. Lett. B **712**, 326 (2012).
[38] O. Hen *et al.* (CLAS Collaboration), Phys. Lett. B **722**, 63 (2013).
[39] T. Mineeva, *Hadronization Studies via Electroproduction off D, C, Fe, and Pb*, Ph.D. thesis, University of Connecticut (2013).
[40] L. W. Mo and Y. S. Tsai, Rev. Mod. Phys. **41**, 205 (1969).
[41] A. Aste, C. von Arx, and D. Trautmann, The European Physical Journal A **26**, 167 (2005).
[42] S. Dasu, P. De Barbaro, A. Bodek, H. Harada, M. Krasny, K. Lang, E. Riordan, L. Andivahis, R. Arnold, D. Benton, *et al.*, Physical Review D **49**, 55204 (1994).
[43] I. Akushevich, N. Shumeiko, and A. Soroko, Eur. Phys. J. C **10**, 681 (1999).
[44] G. Ingelman, A. Edin, and J. Rathsman, Computer Physics Communications **101**, 108 (1997).
[45] C. Ciofi degli Atti and S. Simula, Phys. Rev. C **53**, 1689 (1996).
[46] A. Majumder and M. Van Leeuwen, Prog. Part. Nucl. Phys. **66**, 41 (2011), arXiv:1002.2206 [hep-ph].
[47] J. W. Cronin, H. J. Frisch, M. J. Shochet, J. P. Boymond, P. A. Piroue, and R. L. Sumner, Phys. Rev. D **11**, 3105 (1975).
[48] J. Ashman *et al.* (European Muon Collaboration), Z. Phys. C **52**, 1 (1991).
[49] M. R. Adams *et al.* (E665 Collaboration), Phys. Rev. Lett. **74**, 5198 (1995), [Erratum: Phys.Rev.Lett. 80, 2020–2021 (1998)].
[50] W. K. Brooks *et al.*, "Quark propagation and hadron formation," `https://www.jlab.org/exp_prog/proposals/10/PR12-06-117.pdf` (2010), a CLAS Collaboration proposal.
[51] M. Barabanov *et al.*, Progress in Particle and Nuclear Physics , 103835 (2021).
[52] R. Abdul Khalek *et al.*, Nucl. Phys. A **1026**, 122447 (2022).